Available online at www.sciencedirect.com
ScienceDirect
Vibrational Spectroscopy 44 (2007) 62–68
VIBRATIONAL SPECTROSCOPY
www.elsevier.com/locate/vibspec

Confocal Raman microspectroscopy with dry objectives: A depth profiling study on polymer films

J. Pablo Tomba [a,*], José M. Pastor [b]

[a] Institute of Materials Science and Technology (INTEMA), National Research Council (CONICET), University of Mar del Plata, Juan B. Justo 4302, 7600 Mar del Plata, Argentina
[b] Department of Physics of Condensed Matter, University of Valladolid, Paseo del Cauce s/n, 47011 Valladolid, Spain

Received 25 January 2006; accepted 14 August 2006
Available online 27 October 2006

Abstract

In this work, we test simple models proposed to predict two characteristic features when performing depth profiling with dry-optics confocal Raman microspectroscopy (CRM): the decay in the collected intensity and the degradation of depth resolution with focusing depth due to laser refraction. With this aim, we carried out experiments on transparent thick polystyrene and poly(methyl methacrylate) films, in which we tracked the collected Raman intensity as a function of focusing depth. These results are interpreted in the context of the model proposed by Batchelder. We also investigated the Raman response on a series of well-defined planar interfaces, generated by contact between thin poly(methyl methacrylate) films (45, 94 and 145 μm thickness) coated onto a much thicker piece of poly(butyl methacrylate). These results allowed us to test the enlargement in focus length with focusing depth predicted by the models of Everall and Batchelder. We found that with minor modifications that keep the simplicity of the original treatment, the model of Batchelder reproduces reliably fine features of the Raman intensity profiles. The results of this work show that these simple models cannot only be used to assist data interpretation but also to predict quantitatively Raman intensity variations in depth profiling experiments.

Keywords: Confocal Raman microspectroscopy; Depth profiling; Polymer films; Depth resolution; Dry objectives; Refraction

1. Introduction

Confocal Raman microspectroscopy (CRM) has widely shown to be an invaluable tool in the study of chemical/physical properties of small sample regions. On one hand, the information contained in the Raman spectrum is an essentially unique fingerprint of the material. On the other hand, the use of a point light source in combination with a conjugated pinhole aperture provides spatial discrimination making possible to analyze Raman scattering mostly originated from in-focus planes [1,2]. One of the most attractive features of CRM is the ability to perform in-depth optical sectioning of the sample. In theory, depth (or axial) resolution in confocal conditions is determined by the diffraction-limited laser focal volume, proportional to the laser wavelength and to the inverse square of the numerical aperture of the objective utilized [1]. Experimentally, depth resolution or ‘‘confocality’’ can be measured by scanning through the focus of the microscope objective a material with a sharp edge or feature [3]. In Raman spectroscopy, a flat silicon surface is routinely used with this purpose and the full width at the half maximum of the typical bell-shaped curve obtained gives a measure of the depth of focus in air. This value is routinely informed as the nominal depth resolution of the technique, on the order of 2–5 μm for the objectives and laser wavelengths commonly used.

Several authors have pointed out that optical properties of the sample may affect adversely depth resolution, invoking distortions of the dimensions of the laser spot at the focal point due to scattering, turbidity or refraction [1,4]. However, the work of Everall was the first one in demonstrating that refraction is the main factor of performance degradation, particularly when depth profiling is carried out using the ‘‘dry’’ metallurgical objectives commonly attached to most of the commercial Raman microspectrometers [5,6]. The author modeled and quantified the distortions experienced by the spot illuminated by the laser beam when it is refracted at the

* Corresponding author.
E-mail address: jptomba@fi.mdp.edu.ar (J.P. Tomba).

0924-2031/$ – see front matter © 2006 Elsevier B.V. All rights reserved.
doi:10.1016/j.vibspec.2006.08.001

air/sample interface. One of the most striking consequences of his analysis is that depth resolution can be worsened by orders of magnitude compared with the nominal values determined with silicon wafers, and that deterioration is more severely when one focuses deeper into the sample [5]. It was also shown that the depth scale is artificially compressed by a factor that roughly scales with n, the refractive index of the material [5,6].

One would expect that the pinhole aperture, ignored in the original treatment by Everall, might contribute to partially block out-of-focus scattering helping to improve depth resolution. This problem was addressed by Baldwin and Batchelder, who furnished and excellent and relatively simple description on the role of the pinhole in the collection efficiency of Raman scattering [7]. Their model, in combination with the analysis pioneered by Everall, predicts that although the use of dry optics degrades depth resolution, it is better than that one would expect only based on the axial blurring of the laser beam. The model also predicts a drastic decrease in the collected Raman intensity when probing depth into the sample.

Although the previous treatments give a simple and quite complete view of the problem of laser refraction at the air/sample interface, they only consider on-axis distortions and neglect the influence of laser diffraction. A complete treatment of the problem has been recently considered by Sourisseau and Maraval [8]. Their approach, based on the rigorous vectorial electromagnetic treatment of a similar problem developed by Török et al. [9], accounts for axial and lateral intensity distributions, considers both refraction and diffraction, and includes the pinhole aperture in the calculations. As a counterpart, the mathematical treatment is rather complex and very demanding computationally, requiring about 1 day for carrying out the calculations corresponding to a given depth-profile [8]. The model predicts that off-axis refraction and diffraction reduces the axial broadening of the laser and that depth resolution should remain fairly constant, independently of the focusing depth [8].

Physical sectioning followed by surface analysis or the use of immersion optics has been suggested to minimize the worsening in depth resolution due to laser refraction [5,6]. Whenever these strategies are impractical, the use of models to assist data interpretation becomes crucial. This work is part of a series in which we test models for depth resolution in dry-optics CRM. We focus on the simple theoretical analysis by Everall and the improvements made by Baldwin and Batchelder, as more rigorous treatments are far more complicated and beyond the scope of the work. We start showing experiments that track variations of Raman intensity with focusing depth and pinhole aperture on thick and transparent polymers films. These data are analyzed in the context of the model of Batchelder. Then, we present the Raman response of a series of planar interfaces, generated by contact between two polymer films, which allow us to test the above-mentioned simple approaches for predicting depth resolution. Finally, we consider strategies to improve the model predictions, keeping the simplicity of the original treatments.

2. Theoretical

In this section, we summarize the highlights of the models of Everall [5] and Baldwin and Batchelder [7]. Based on simple ray-tracing analysis, the models predict the path of the laser beam when it passes through the air/sample interface. In depth profiling, one focus the laser beam at a nominal point Δ from the air/sample surface, according with the scale of the microscope platform. The laser emerges from the lens pupil as a series of rays that travel by air and are refracted at the sample surface, with refractive index n, according to the Snell's law. The distance across the microscope is normalized in terms of the pupil parameter m; while $m = 0$ corresponds to normal incident rays, $m = 1$ corresponds to rays with the maximum incident angle, limited by the numerical aperture (NA) of the microscope objective used [5]. Due to refraction, the infinitesimal laser spot, originally directed at the point Δ, is spread in a range of z values between $z_{\min}(m = 0)$ and $z_{\max}(m = 1)$. According to Everall, z and Δ are related as:

$$z = \Delta\left[m^2\frac{\mathrm{NA}^2(n^2-1)}{1-\mathrm{NA}^2}+n^2\right]^{1/2} \quad (1)$$

It is considered that the laser intensity has a Gaussian distribution intensity along the pupil lens, $I(m)$, that illuminates the $z_{\min} - z_{\max}$ region with a radial distribution, proportionally to the product $mI(m)$. The distribution of laser intensity in axial direction $I_d(m)$ is then expressed as:

$$I_d(m) = mI(m) = mI_0\exp(-2m^2) \quad (2)$$

where I_0 is the incident axial intensity. The models assume that the laser illuminates only the optical axis (z) and that orthogonal spreading is negligible. To calculate the collected Raman intensity, the treatment of Everall either ignores the pinhole or considers that the device works perfectly [5]. The collected Raman intensity over $z_{\min} - z_{\max}$ (R^{Ev}) is calculated assuming the same weighting factor for the probability than that used in the illumination path (m),

$$R^{\mathrm{Ev}}(z) = mI_d(m) \quad (3)$$

recalling that z depends on m through Eq. (1). Fig. 1 shows the collected Raman intensity (solid lines) as a function of the true focal position (z) for three values of nominal focal positions (Δ), as predicted by Everall. For the simulations we used NA = 0.90 and $n = 1.5$. The areas under the curves have been normalized to unity.

Fig. 1 illustrates the effect of laser refraction on depth resolution. Raman scattering is collected over an increasingly wider region that lies much deeper than the nominal point where the laser beam was originally focused (Δ). These regions are extended over distances on the order of tens of micrometers, much larger than the diffraction-limited depth of focus.

Baldwin and Batchelder [7] refined the treatment of Everall considering that in the collection path the confocal system blocks some of the refracted rays restricting the fraction of illuminated region from which Raman scattering is primary detected. The authors modeled the effect of the air/sample interface on the

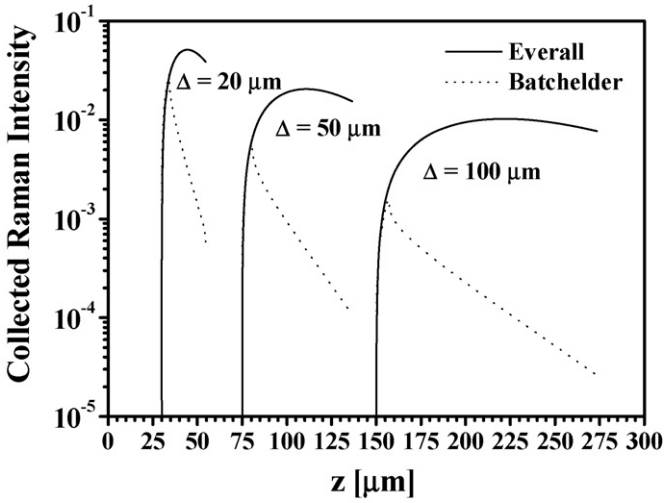

Fig. 1. Depth resolution curves for three values of the nominal focusing depth (Δ), as predicted by Everall (solid lines) and Batchelder (dotted lines). Simulations were carried out with NA = 0.9, n = 1.5 and ρ = 1.738.

collection aperture of the confocal system and calculated, for each axial illuminated spot, how much of the Raman scattered light is allowed to pass by a confocal back aperture of radius ρ. The efficiency of the confocal system is expressed in terms of the collection solid angle (Ω) for each illuminated point along z. It was shown that the collection efficiency has in most of cases two distinct regimes. Near to the air/sample interface, there is a circular acceptance aperture whose angular size increases as the illuminated point is moved away from the interface. At larger depths, a forbidden annulus, whose thickness grows rapidly with focusing depth, increases in significance and reduces the collected intensity [7]. As a result, $\Omega(z)$ has a peaked shape. Following Batchelder, the collected Raman intensity including the effect of the pinhole aperture on the ray trace, is:

$$R^{\mathrm{Bt}}(z_m) = I_{\mathrm{d}}(m)\Omega(\Delta, n, \mathrm{NA}, \rho) \quad (4)$$

For details about the numerical methods employed to calculate $\Omega(\Delta, n, \mathrm{NA}, \rho)$ see Ref. [7].

The predictions of the model of Batchelder are shown in Fig. 1 with dotted lines, for values of NA = 0.9 and n = 1.5. Briefly, the calculation procedure consists in first calculating the normalized distribution of illumination along z using Eq. (2) and, for each of these points, Ω, the collection solid angle. Then, the Raman response is calculated using Eq. (4). For the simulations shown in Fig. 1, we used ρ = 1.786 μm, a typical value for confocal radius, as will be shown later. The model predicts a decrease in the collected intensity with increasing depth and a sharper overall response with depth compared with Everall's prediction. The peaked shape of the $\Omega(z)$ curves concentrates the sampled region into a smaller volume than that predicted in absence of pinhole.

3. Experimental

The polymers used to prepare films, poly(methyl methacrylate) (PMMA), poly(n-butyl methacrylate) (PBMA) and polystyrene (PS), were obtained from Aldrich. The oil used as immersion fluid (n = 1.5, from Merck, catalogue number B446082) was supplied by the microscope objective manufacturer (Olympus). Polymer films with thicknesses in the range 10–1000 μm were prepared by standard vacuum molding techniques, as detailed elsewhere [10]. Thick films of PS and PMMA were used in the experiments as obtained. In the experiments with bi-layer polymer films, the thin rigid polymer (PMMA) was molded first at the desired thickness (10–200 μm), measured with a linear optical encoder at 1 μm resolution, and then put in contact onto the soft and thick, previously molded, PBMA layer.

Raman spectra were recorded at room temperature, on a Raman microspectrometer DILOR LabRam Confocal, equipped with a 16-mW He–Ne laser beam (632.8 nm wavelength). A slit opening of 500 μm and a holographic grating of 1800 lines/mm were used, rendering a spectral resolution of 5 cm^{-1}. We used a dry Olympus 100× objective (NA = 0.9, 210 μm working distance) in combination with variable pinhole openings (the maximum aperture is 1000 μm). Some measurements were also carried out with an immersion Olympus 100× objective (NA = 1.3, 210 μm working distance). For depth profiling, the samples were mounted on a microscope stage with vertical displacement (z-axis) controlled manually with the micrometric screw of the microscope. Raman intensity depth-profiles were measured by taking Raman spectra from different depths, moving the stage vertically (z) in steps of 1–5 μm. To compute the Raman intensity of individual components, we applied the linear decomposition method [11]. The technique reconstructs the composite spectra from the spectra of individual components, measured independently, and evaluates the relative contribution of each of them to the global spectrum.

4. Results and discussion

4.1. Effect of focusing depth on the collection efficiency

Fig. 2A–C shows Raman intensity depth-profiles obtained from a series of thick and transparent polymer films. Raman intensities were calculated from the relative contribution of individual components to the global spectrum, as obtained after applying the linear decomposition method [11]. The depth scale corresponds to the nominal focusing depth (Δ) as determined from the micrometric screw of the microscope, where the zero corresponds to the sample surface. The maximum depth probed is limited by the working distance of the objective (210 μm).

Fig. 2A shows Raman intensity depth-profiles on a PMMA 1 mm thick film, scanned through air, using a ×100 metallurgical objective (NA = 0.9) in combination with different confocal apertures (300, 500 and 800 μm), as set in the software of the LabRam instrument. Fig. 2B shows similar results for a 1 mm thick PS sample. Fig. 1C corresponds to the same PS sample studied with a ×100 immersion objective, through a medium that matches almost exactly the refractive index of the polymer. We scanned all these films focusing the microscope 20 μm above the sample surface, and then moving

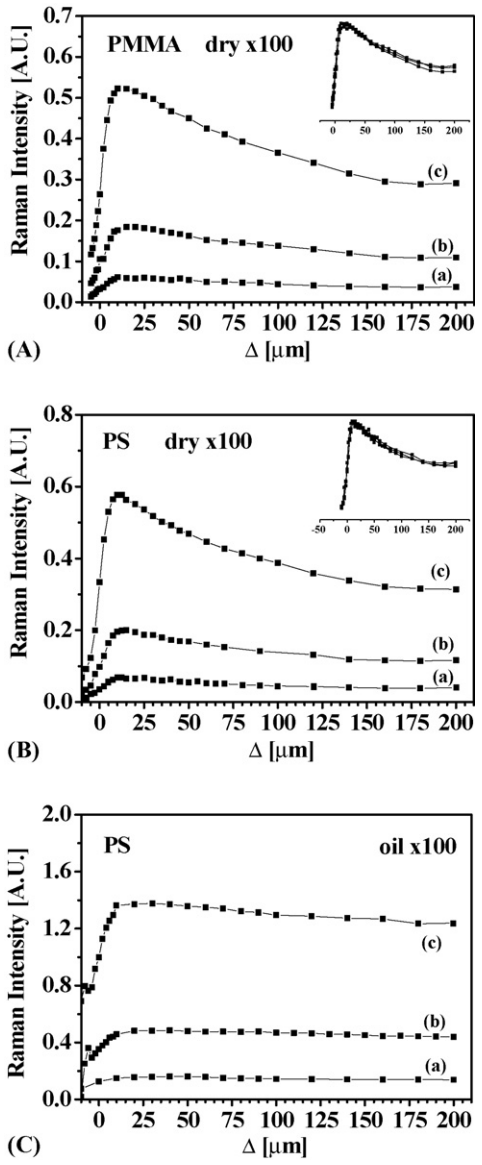

Fig. 2. Raman intensity profiles on thick and transparent polymer films, for different pinhole apertures: (a) Φ = 300 μm; (b) Φ = 500 μm; (c) Φ = 800 μm. (A) PMMA film studied with a dry ×100 objective. (B) PS sample studied with a dry ×100 objective. (C) PS sample studied with an immersion objective and a coupling fluid with $n = 1.5$. The insets in figs. (A) and (B) show the Raman intensity curves normalized.

the focal point in the sample direction. For this reason, Raman intensity starts from a value near to zero, when the focal volume is in air, and rapidly increases when the focal point passes through the sample surface and finally reach the sample. After this rapid increase, Raman intensity decreases as the focal point is displaced below the sample surface and deeper into the sample.

One observes that the collected Raman intensity decreases markedly with focusing depth only in those samples studied with dry objectives. Both PS and PMMA samples show the same decay rate, with profiles nearly identical. Remarkably, the fall in Raman intensity is practically absent when PS was examined with immersion objectives, as shown in Fig. 2C. The fall of Raman intensity has been systematically reported in depth profiling experiments with dry objectives and sometimes attributed to sample absorption or scattering effects [1,12]. Here, and providing both samples are transparent and perfectly homogeneous, one have to look for a factor other than those mentioned. Baldwin and Batchelder were the first to describe the effect of laser refraction at the air/sample interface on the collection efficiency of the confocal system [7]. The authors modeled the distortions of the scattering volume defined by the confocal aperture, which results in a continuous reduction with depth of the number of Raman photons that reach the detector. Notice that the effect is not predicted by Everall as his model does not consider the presence of the pinhole on the collection path of the laser beam.

In the context of the analysis by Batchelder, the collection efficiency for each Δ value can be calculated by integrating Eq. (4) along z_m. In Fig. 3, we compare experimental results corresponding to the PMMA sample with the fall in collection efficiency predicted by Batchelder. For computational simulations, we used NA = 0.9 and a PMMA refractive index of 1.49. The radius of the confocal aperture defined in the model of Batchelder (ρ) was related with the nominal pinhole aperture set in our microspectrometer (Φ) in the following way. In LabRam instrument, the pinhole is squared and the value one set in the software corresponds to the diagonal of the square in micrometer. The magnification between the sample and the confocal hole is the microscope magnification (M) multiplied by a factor of 1.4 [13]. For example, a hole of 280 μm used with a ×100 objective corresponds to a sampled area of 2 μm. Thus, the pinhole aperture is approximately related with the radius of the virtual image of the confocal aperture in the focal plane (ρ) as $\Phi = 1.4M\,2\rho$. The simulations in Fig. 3 were carried out with $\rho = 1.786$ μm, corresponding to $\Phi = 500$ μm as set in the LabRam software.

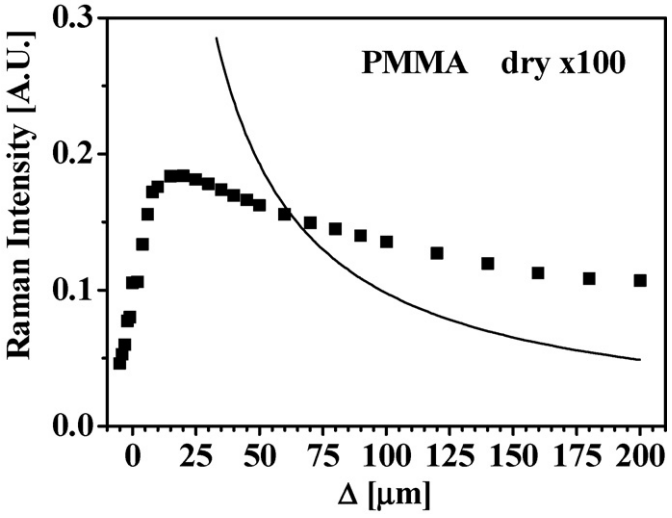

Fig. 3. Experimental confocal Raman response as a function of the nominal focusing depth (symbol) compared with that predicted by Batchelder (solid line) for the PMMA sample studied under a dry ×100 objective and Φ = 500 μm.

We see that, even though the model prediction is qualitatively correct, it largely overestimates the fall rate of Raman scattering, particularly at low depth values. This problem has also been reported by other authors (see Ref. [14]), contrasting with the results reported in the original work of Batchelder, where model predictions fit well the experimental data obtained by depth profiling a piece of diamond [7]. One possible reason of the discrepancy might be that the comparison was carried out over a much larger range of depth values (1500 μm) than that of this work. It is worthwhile to mention that the complete treatment of the problem presented by Sourisseau and Maraval in Ref. [8] predicts quite well the decays curves in the range 0–200 μm but employing a much more complex mathematics.

It is interesting to analyze the effect of the pinhole aperture on the decay curves. We observed that the variations in Raman intensity scale with the square of Φ, the size of the pinhole aperture, in any of the cases analyzed through Fig. 2A–C. It agrees with what one would expect for light transmitted through a hole that changes its aperture surface [1]. Although the model of Batchelder has been solved considering the pinhole as a two dimensional aperture, the predicted dependence of Raman intensity with pinhole diameter is linear. Other authors have also reported a linear relationship between Raman intensity and Φ, but without analyzing the possible reasons [14]. Clearly, the problem is not trivial and requires further study. We also observe that, when normalized, the shape of the intensity profiles is independent of the confocal aperture, as seen in the insets of Fig. 2A and B. The way that these effects are related with depth resolution will be analyzed in the next section.

4.2. Raman response of planar interfaces

The results shown in Fig. 1 represent the depth resolution curves predicted by the models when CRM is operated with traditional dry objectives. One of the ways to test these predictions is by measuring the Raman response on samples with well-defined composition profiles. In this case, the actual instrumental response will be a convolution of the depth resolution curves with the sample composition profile. We focus our analysis on planar polymeric interfaces, generated by coating a thin PMMA film onto a soft and relatively thick PBMA layer. As PMMA is glassy at room temperature, good physical contact with the soft PBMA film can be achieved just by pressing the films under a moderate pressure. At the same time, diffusion between films is negligible and the interfaces are characterized by well-defined step-like composition profiles.

In Fig. 4A and B, we simulated the expected Raman response of a planar interface between a 145 μm PMMA film and a thick PBMA layer, as predicted by Everall (dotted lines) and Batchelder (dashed lines). The curves were obtained by solving the corresponding convolution integral between a step profile and the depth resolution curves generated by the models. The refractive indexes of PMMA and PBMA are 1.489 and 1.483, respectively [15]; for computational simulations, we assumed a homogeneous medium with $n = 1.485$ along with NA = 0.9 and $\Phi = 500$. Fig. 4A corresponds to the Raman response of the PMMA film while Fig. 4B shows the PBMA layer profile, as

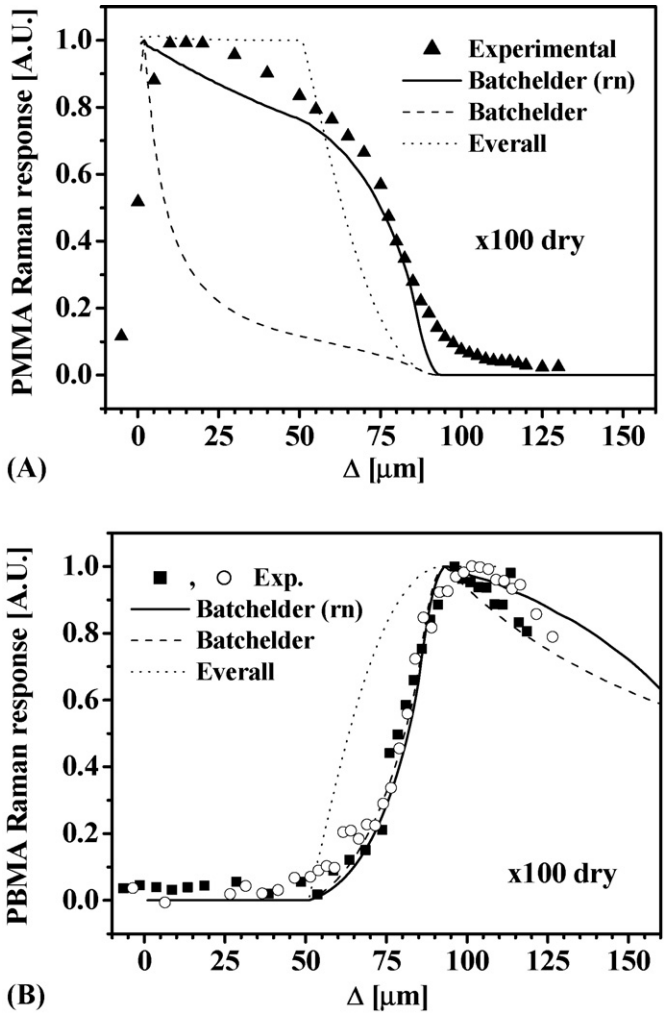

Fig. 4. Experimental and predicted Raman response of planar PMMA/PBMA interfaces. rn refers to the response calculated after renormalization, as detailed in the text. (A) PMMA film and (B) PBMA layer as measured through the PMMA film. Objective used: dry ×100 (NA = 0.9); open symbols refer to Φ = 300 μm; solid symbols to Φ = 500 μm.

measured through the PMMA film. The zero in the depth scale corresponds to the air/PMMA interface. For comparison purposes, we have also included experimental results (circles) obtained from depth profiling experiments with a dry objective through a 145 μm PMMA film coated onto a PBMA layer.

As demonstrated in his original work, the model of Everall predicts the main features of the experiment (see Fig. 4A): (a) the PMMA layer, 145 μm thick, appears artificially thinned due to refraction aberrations, by a factor that roughly scales with the refractive index of the medium; (b) the interlayer transition, expected to be very sharp, is extended over a quite broad region. However, the model does not account for the fall in Raman intensity with focusing depth and fail in reproducing the detailed shape of the Raman profile, overestimating the apparent compression in the depth scale. As observed in Fig. 4B, this issue is partially solved with the improvements introduced by Batchelder, which essentially shift the collection volume at higher depths (see Fig. 1). In this case, the lack of precision in predicting the fall rate in Raman intensity,

discussed in the previous section, is counterbalanced by the sudden increase in Raman intensity that occurs when the focal volume passes through the interface and the overall prediction is remarkably close to the experimental data. However, the problem becomes evident in Fig. 4A. The tails in the intensity profiles observed in the range 90–125 μm are most likely due to factors others than refraction (i.e. diffraction, instrumental) that contribute to make the profile broaden. These effects are obviously not accounted by the models considered here that only address broadening by refraction.

To exemplify the effect of the size of the pinhole aperture on the intensity profiles, we have included in Fig. 4B experimental data obtained with two different Φ values (500 and 300 μm). Remarkably, we do not observe substantial improvements in depth resolution by reducing the size of the confocal hole. The shape of the experimental PBMA Raman responses is nearly independent of Φ, in agreement with the already observed good superposition in the intensity decay curves obtained with different Φ values seen in Fig. 2A and B. These observations can be rationalized in the context of the model of Batchelder, which, indeed, predicts depth resolution curves rather independent of ρ [7]. Depth resolution is mainly determined by the relative collection efficiency for marginal ($m \sim 0$) and paraxial ($m \sim 1$) illuminated points [5,7]. The contribution from marginal points will change slowly with the size of the confocal aperture because the collection solid angle split into the paraxial disk and the outer annulus. The size of both of these allowed return paths scales with confocal aperture, as does the size of the paraxial disk on the collection path for a paraxial illumination point [7]. Hence, the ratio of the collected intensities from paraxial and marginal illuminated regions is not strongly dependent on the size of the confocal aperture and the main effect of this parameter is to change the overall collected intensity.

4.3. Improvements in the model predictions

Although the model of Batchelder does not reproduce quantitatively the fall in Raman intensity, it certainly has success in predicting the effective depth of focus and consequently the apparent position of the planar interface, as shown in Fig. 4B. A simple way to correct the first problem is to incorporate in the calculations information from independent experiments of collection efficiency as a function of depth, through renormalization of the depth resolution curves predicted by Batchelder in Fig. 1. Briefly, the area of each depth resolution curve for a given value of nominal depth is multiplied by the experimentally observed Raman intensity at this point, as taken from Fig. 2A and B. As the PBMA sample is transparent and homogeneous, we considered the same intensity decay rate in that material that in PMMA. Then, this family of corrected curves is used to calculate the corresponding convolution integrals. Examples of such corrections are given in Fig. 4, with solid lines. We see that the details of the Raman profile are now correctly reproduced, except for the above-mentioned tails due to diffraction/instrumental factors not accounted by the models.

To test more carefully this strategy, we examined a series of PMMA/PBMA planar interfaces positioned at different depths, through the use of PMMA films with a range of thicknesses (45, 94 and 145 μm). We measured first the Raman profiles of the PMMA/PBMA interfaces with immersion optics through a medium that matches the refractive index of the polymer sample, using coupling oil between the microscope objective and the PMMA surface. Fig. 5 shows the PMMA Raman response for the three systems examined. We observe that the interfaces appear located at depths very close to the nominal thickness values of the PMMA films, showing that the oil used as immersion fluid effectively minimizes the differences in refractive index between medium and sample and the consequent deviation of the laser beam at the PMMA surface. No decay in Raman intensity throughout the PMMA films is observed. The originally planar interfaces appear broadened in the same degree for the three cases. The effect can be safely attributed to blurring by diffraction/instrumental factors, typically invariant with focusing depth [17,16].

These profiles represent a very close approximation to the Raman response in absence of refraction. To simulate the instrumental response more realistically, we use these profiles, instead of the theoretical expected step-functions, to calculate the corresponding convolution integrals. These calculations should yield the expected Raman response due to combined effects of refraction and diffraction/instrumental factors. Results of the predicted response are shown in Fig. 6A and B (solid lines) along with experimental results (symbols) obtained from depth profiling experiments through the PMMA film with a ×100 dry objective. In Fig. 6A, we show the Raman response of the PMMA layer while Fig. 6B shows the Raman response corresponding to the PBMA layer. We see that the predicted Raman response is very close to that measured for both PMMA and PBMA films. The decay rate of Raman intensity, the apparent position of the interface, and its broadness are very well reproduced for the three PMMA films studied. Artificial tails, produced by refraction of the blurred interfaces used in the convolution integrals, reproduce precisely those observed in the experimental data. Notice that the range

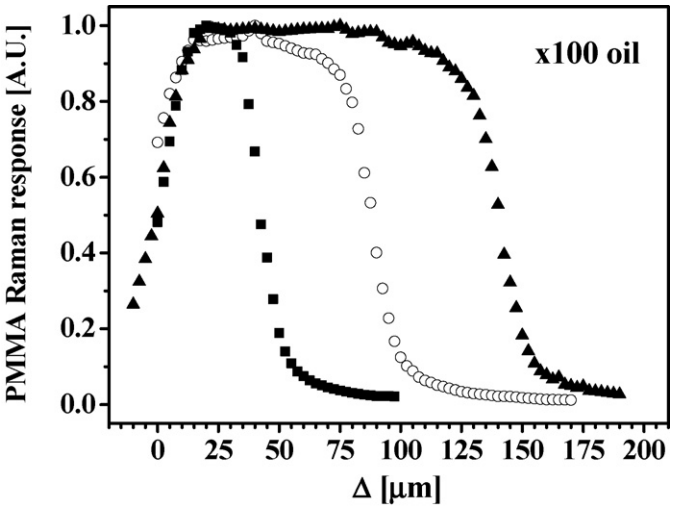

Fig. 5. Raman intensity profiles for three PMMA/PBMA planar interfaces, examined with immersion optics through the PMMA layer. Thicknesses of the PMMA films were 45, 94 and 145 μm and Φ = 500 μm.

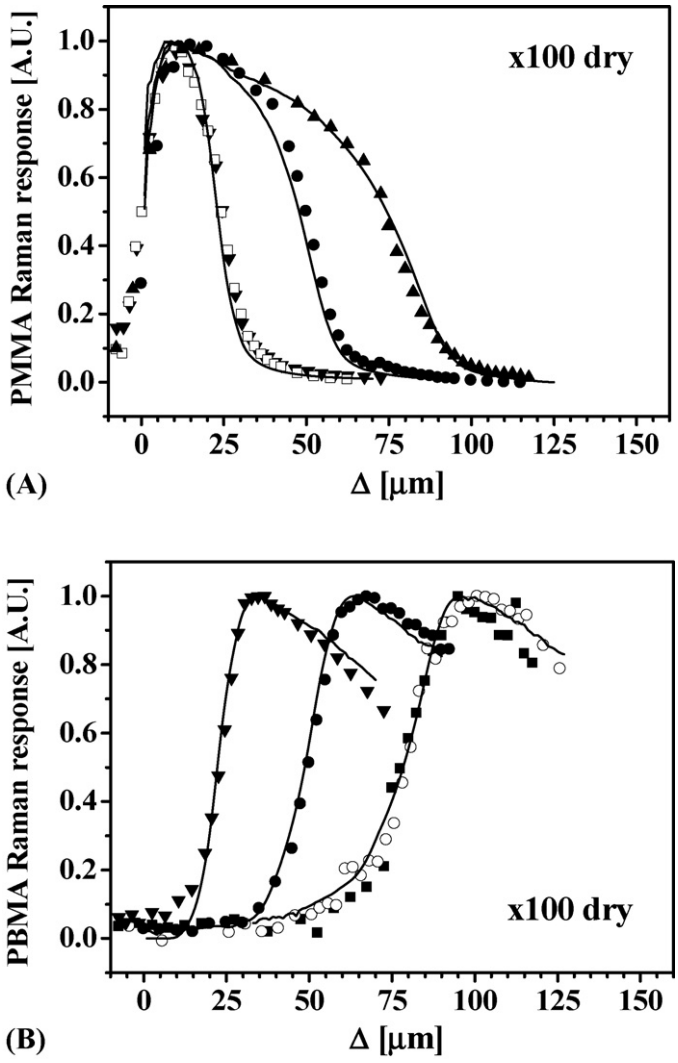

Fig. 6. Raman intensity profiles of planar interfaces measured with dry optics. (A) PMMA Raman response and (B) PBMA Raman response. Objective used: dry ×100 (NA = 0.9); open symbols refer to Φ = 300 μm; solid symbols to Φ = 500 μm.

of depths analyzed covers quite completely the operative range for the microscope objective used (210 μm). Small differences may be attributed to the fact that dry and immersion objectives were different and the broadening due to diffraction/instrumental factors observed in Fig. 5 may not be the same that those corresponding to the data of Fig. 6. Nevertheless, and given the simplicity of the approach used, the agreement between model predictions and experimental data is remarkable.

5. Conclusions

We have tested a series of simple models that predict the degradation of depth resolution by laser refraction in dry-optics CRM experiments. Although the model of Batchelder represents a step forward with respect to the original work of Everall, it overestimates the decay rate in efficiency collection associated with the pinhole aperture and the model fails in reproducing the detailed shape of Raman response in experiments with planar interfaces. One would expect that the resulting improvement in depth resolution was also overestimated compared with the original predictions by Everall; however, the model predicts quite well the observed depth resolution and the apparent compression in the depth scale. It suggests that other effects not accounted by these simple models, such as off-axis intensity contributions, may effectively operate to further improve depth resolution, as pointed out by other authors [8]. The renormalization of the depth resolution curves with the experimentally observed intensity decay rates yielded a much better match to the experimental data. Overall, the strategy improved the prediction capabilities of the models and could account for fine details of the Raman intensity profiles in a wide range of depths.

Although other authors have solved the problem with higher levels of rigor and sophistication, these simple models for depth resolution have shown to be not only a valuable tool to assist data interpretation, but also to reproduce quantitatively the most important features of the experiments. Strategies aimed at generalizing this simple approach should face at least two important problems: a reliable characterization of other sources of artificial broadening such as diffraction/instrumental factors, either theoretically [16] or experimentally [17], and the study of opaque samples, where intensity decay rates are not only related with refraction. These issues will be addressed in a forthcoming publication.

Acknowledgments

J.P. Tomba would like to thank Department of Chemistry of University of Toronto for the preparation of samples and Drs. L. Izaguirre and M. Herguedas for their valuable assistance during CRM measurements. This project was funded by CYTED (project VIII.11).

References

[1] R. Tabaksblat, R.J. Meier, B.J. Kipp, Appl. Spectrosc. 46 (1992) 60.
[2] G.J. Puppels, F.F.M. de Mul, C. Otto, J. Greve, M. Robert-Nicoud, D.J. Arndt-Jovin, T.M. Jovin, Nature 347 (1990) 301.
[3] G.P. Puppels, W. Colier, J.H.F. Olminkhof, C. Otto, F.F.M. de Mul, J. Greeve, J. Raman Spectrosc. 22 (1991) 217.
[4] S. Hajatdoost, M. Olsthoorn, J. Yarwood, Appl. Spectrosc. 51 (1997) 1784.
[5] N. Everall, Appl. Spectrosc. 54 (2000) 1515.
[6] N. Everall, Appl. Spectrosc. 54 (2000) 773.
[7] K.J. Baldwin, D.N. Batchelder, Appl. Spectrosc. 55 (2001) 517.
[8] C. Sourisseau, P. Maraval, Appl. Spectrosc. 57 (2003) 1324.
[9] P. Török, P. Varga, G. Németh, J. Opt. Soc. Am. A 12 (1995) 2660.
[10] J.P. Tomba, J.M. Carella, J.M. Pastor, Macromolecules 38 (2005) 4355.
[11] J.P. Tomba, E. de la Puente, J.M. Pastor, J. Polym. Sci.; Part B: Polym. Phys. 38 (2000) 1013.
[12] S. Hajatdoost, J. Yarwood, Appl. Spectrosc. 57 (2003) 1324.
[13] LabRam Manual, Jobin Yvon-HORIBA, France, 1995.
[14] J.L. Brunnel, J.C. Lassegues, C. Sourisseau, J. Raman Spectrosc. 33 (2002) 815.
[15] J. Brandrup, E.H. Immergut, E.A. Grulke, Polymer Handbook, J. Wiley & Sons, 1999.
[16] L. Baia, K. Gigant, U. Posset, R. Petry, G. Schottner, W. Kiefer, J. Popp, Vib. Spectrosc. 29 (2002) 245.
[17] J. Vyorykka, J. Paaso, M. Tenhunen, H. Iitti, T. Vuorinen, P. Stenius, Appl. Spectrosc. 57 (2003) 1123.